A boundary perturbation method for recovering interface shapes in layered media

2011 Inverse Problems 27 095009

(http://iopscience.iop.org/0266-5611/27/9/095009)

Inverse Problems **27** (2011) 095009 (18pp) doi:10.1088/0266-5611/27/9/095009

A boundary perturbation method for recovering interface shapes in layered media

Alison Malcolm[1] **and David P Nicholls**[2]

[1] Department of Earth, Atmospheric, and Planetary Sciences, Massachusetts Institute of Technology, Cambridge, MA 02139, USA
[2] Department of Mathematics, Statistics, and Computer Science, University of Illinois, Chicago, IL 60607, USA

E-mail: davidn@uic.edu

Received 4 May 2011, in final form 14 July 2011
Published 16 August 2011
Online at stacks.iop.org/IP/27/095009

Abstract
The scattering of linear acoustic radiation by a periodic layered structure is a fundamental model in the geosciences as it closely approximates the propagation of pressure waves in the earth's crust. In this contribution, the authors describe new algorithms for (1) the forward problem of prescribing incident radiation and, given the known structure, determining the scattered field, and (2) the inverse problem of approximating the form of the structure given prescribed incident radiation and measured scattered data. Each of these algorithms is based upon a novel statement of the problem in terms of boundary integral operators (Dirichlet–Neumann operators), and a boundary perturbation algorithm (the method of operator expansions) for their evaluation. Detailed formulas and numerical simulations are presented to demonstrate the utility of these new approaches.

1. Introduction

The interior of the earth's crust can effectively be modeled as a layered media: largely homogeneous blocks of material separated by sharp interfaces across which material properties change discontinuously. With such a model in mind, one can pose two important and related questions. (1) Given the knowledge of the material properties of the layers and the shapes of the interfaces, can one compute scattering returns from such a structure given incident radiation? (2) Specifying incident radiation and measuring scattered waves, can one deduce information about material properties and interface shapes within the layered media? In this paper, we take up both questions (the 'forward' problem (1) and the 'inverse' problem (2)) and propose novel algorithms for each. These algorithms are based upon a new formulation of the problem in terms of Dirichlet–Neumann operators (DNOs), and convenient boundary perturbation (BP) formulas for their simulation.

Unsurprisingly, the full complement of classical numerical methods have been brought to bear upon both the forward and inverse problems we mention above. The finite difference method (FDM) [MRE07, Pra90], finite element method (FEM) [Zie77, KFI04] and spectral element method (SEM) [KT02a, KT02b] have been implemented but suffer from the fact that they discretize the full volume of the model incurring significant cost, and the difficulty of faithful enforcement of far-field boundary conditions. A compelling alternative are *surface* methods [SSPRCP89, Bou03] (e.g. boundary integral methods or boundary element methods) which only require a discretization of the layer *interfaces* (rather than the whole structure) and which, due to the choice of Green's function, enforce the far-field boundary condition exactly. However, these methods, while capable of delivering high-accuracy solutions, must not only utilize specially designed quadrature rules which respect the singularities in Green's function, but also generate a dense system of linear equations to be solved which require carefully designed preconditioned iterative methods (with accelerated matrix-vector products, e.g., by the fast-multipole method [GR87]).

The literature on methods for the inverse problem is as vast as that for the forward problem, occupying hundreds of books and thousands of papers (the text of Colton and Kress [CK98] is an excellent starting point). Interestingly, most of the work has concerned the bounded-obstacle problem, but for the recovery of interface shapes in layered media we point out some recent work based upon classical integral formulations and the solution of the resulting (nonlinear and ill–conditioned) equations [KT00, AKY06, CG11]. For a more extensive review, we refer the interested reader to the bibliographies of these.

Here we propose a boundary perturbation method for both the forward and inverse problems for irregularly shaped periodic layered media. Like boundary integral/equation methods, our approach requires only the discretization of the layer interfaces while it avoids not only the need for specialized quadrature rules but also the solution of dense linear systems. Our approach is a generalization of the 'method of operator expansions' (OE) of Milder [Mil91a, Mil91b, MS91, MS92, Mil96b, Mil96a] which we use precisely because the interface shapes appear so *explicitly* in these formulations making them particularly appealing for the development of an inversion algorithm. For a generalization of the closely related 'method of field expansions' (FE) described by Bruno and Reitich [BR92, BR93a, BR93b, BR93c] for dielectric structures with multiple layers (denoted there the 'method of variation of boundaries'), we refer the interested reader to the authors' recent publication [MN11].

As with the OE method as it was originally designed by Milder, our new approach is spectrally accurate (i.e. has convergence rates faster than any polynomial order) due to both the analyticity of the scattered fields with respect to boundary perturbation and the optimal choice of spatial basis functions which arise naturally in the methodology. Our inversion strategy is inspired by the work of Nicholls and Taber [NT08, NT09] on the recovery of topography shape under a layer of an ideal fluid (e.g. the ocean) which also uses the *explicit* nature of the OE formulas to great effect.

The organization of the paper is as follows. In section 2, we recall the governing equations. In section 3, we discuss considerations of the forward problem, including a new algorithm for the forward problem (section 3.1) and formulas for Taylor series coefficients of the relevant boundary operators (sections 3.2, 3.3 and 3.4). We also present the exact formula in the flat interface case (section 3.5) and a representative numerical result for a non-trivial interface (section 3.6). In section 4, we outline our new methods for solving the inverse problem, including both an iteration-free (linear) algorithm (section 4.1) and an iterative (nonlinear) method (section 4.2); numerical results are presented in section 4.3.

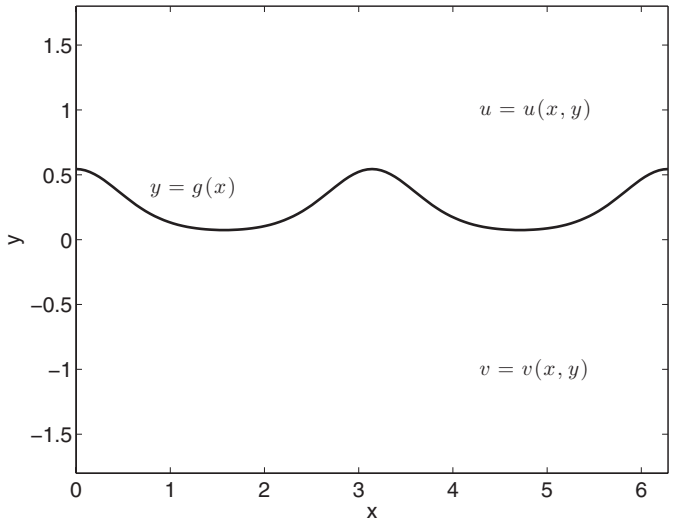

Figure 1. Problem configuration with a layer boundary (solid line); here, $g(x) = 0.2\exp(\cos(2x))$.

2. Governing equations

It is well known that the (reduced) scattered pressure inside a d-periodic structure satisfies the Helmholtz equation with illumination conditions at the interface, and outgoing wave conditions at positive and negative infinity. More precisely, we define the domains

$$S_u = \{(x, y) \mid y > g(x)\}, \qquad S_v = \{(x, y) \mid y < g(x)\}, \qquad g(x + d) = g(x)$$

with the (upward pointing) normal

$$N = (-\partial_x g, 1)^T;$$

see figure 1.

Both domains are constant-density acoustic media with velocities c_j $(j = u, v)$; we assume that plane-wave radiation of wavenumber $(\alpha, -\beta) = (\alpha, -\beta_u)$ is incident upon the structure from above:

$$\mathbf{u}(x, y, t) = \mathrm{e}^{-\mathrm{i}\omega t}\,\mathrm{e}^{\mathrm{i}(\alpha x - \beta_u y)} = \mathrm{e}^{-\mathrm{i}\omega t} u_i(x, y). \tag{2.1}$$

With these specifications, we can define in each layer the parameter $k_j = \omega/c_j$ which characterizes both the properties of the material and the frequency of radiation in the structure. If the reduced scattered fields (i.e. the full scattered fields with the periodic time dependence factored out) in S_u and S_v are respectively denoted $\{u, v\} = \{u(x, y), v(x, y)\}$, then these functions will be quasiperiodic [Pet80]

$$u(x + d, y) = \mathrm{e}^{\mathrm{i}\alpha d} u(x, y), \qquad v(x + d, y) = \mathrm{e}^{\mathrm{i}\alpha d} v(x, y),$$

and the system of partial differential equations to be solved are

$$\Delta u + k_u^2 u = 0 \qquad y > g(x) \tag{2.2a}$$

$$\mathcal{B}\{u\} = 0 \qquad y \to \infty \tag{2.2b}$$

$$\Delta v + k_v^2 v = 0 \qquad y < g(x) \tag{2.2c}$$

$$\mathcal{B}\{v\} = 0 \qquad y \to -\infty \tag{2.2d}$$

$$u - v = \zeta, \qquad \partial_N(u - v) = \psi \qquad y = g(x), \tag{2.2e}$$

where

$$\zeta(x) := -u_i(x, g(x)) = -\mathrm{e}^{\mathrm{i}(\alpha x - \beta_u g(x))} \tag{2.2f}$$

$$\psi(x) := -[\partial_N u_i(x, y)]_{y=g(x)} = (i\beta_u + i\alpha(\partial_x g))\,\mathrm{e}^{\mathrm{i}(\alpha x - \beta_u g(x))}. \tag{2.2g}$$

In these equations, the operator $\mathcal{B}$ enforces the condition that scattered solutions must either be 'outgoing' (upward in S_u and downward in S_v) if they are propagating, or 'decaying' if they are evanescent. We make this 'outgoing wave condition' (OWC) [Pet80] more precise in the Fourier series expression for the exact solution, see (2.3) below.

The quasiperiodic solutions of the Helmholtz equations—(2.2*a*) and (2.2*c*)—and the OWCs—(2.2*b*) and (2.2*d*)—are given by [Pet80]

$$u(x, y) = \sum_{p=-\infty}^{\infty} a_p \exp(\mathrm{i}(\alpha_p x + \beta_{u,p} y)) \tag{2.3a}$$

$$v(x, y) = \sum_{p=-\infty}^{\infty} b_p \exp(\mathrm{i}(\alpha_p x - \beta_{v,p} y)), \tag{2.3b}$$

where the OWC mandates that we choose the positive sign in front of $\beta_{u,p}$ in (2.3*a*) and the negative sign in front of $\beta_{v,p}$ in (2.3*b*). These formulas are valid provided that (x, y) are *outside* the grooves, i.e.

$$(x, y) \in \{y > |g|_{L^\infty}\} \cup \{y < -|g|_{L^\infty}\}.$$

In these equations

$$\alpha_p = \alpha + (2\pi/d)\,p, \qquad \beta_{j,p} = \begin{cases} \sqrt{k_j^2 - \alpha_p^2} & \alpha_p^2 < k_j^2 \\ i\sqrt{\alpha_p^2 - k_j^2} & \alpha_p^2 > k_j^2 \end{cases}, \tag{2.4}$$

where $j = u, v$ and d is the period of the structure. Again, the OWC determines the choice of sign for $\beta_{j,p}$ in the evanescent case $\alpha_p^2 > k_j^2$.

3. Forward problem

For the forward problem, we specify the grating $g(x)$ and the Dirichlet and Neumann data from the incident radiation: $\zeta(x)$ and $\psi(x)$. From this we should produce the scattered fields $u(x, y)$ and $v(x, y)$. However, it is not difficult to deduce that if we recover the Dirichlet and Neumann traces of u and v

$$U(x) := u(x, g(x)), \qquad V(x) := v(x, g(x)),$$
$$U'(x) := (\partial_N u)(x, g(x)), \qquad V'(x) := (\partial_N v)(x, g(x)),$$

then integral formulas will give us u and v everywhere.

Furthermore, if we define the Dirichlet–Neumann operators (DNOs) as

$$G(g)[U(x)] := U'(x), \qquad H(g)[V(x)] := V'(x),$$

then it suffices to find simply the Dirichlet traces U and V. As the DNOs encapsulate the solution of the Helmholtz equations and the OWCs, it is not difficult to see that (2.2) are equivalent to the *surface* equations

$$U - V = \zeta \tag{3.1a}$$

$$G[U] - H[V] = \psi. \tag{3.1b}$$

This can be simplified in a number of ways, but one which is convenient for our current purposes uses the first equation to solve for V, $V = U - \zeta$, which is then inserted into the second equation yielding

$$(G - H)[U] = \psi - H[\zeta]. \tag{3.2}$$

As the boundary quantity U will be inconvenient or impossible to recover, we note that an alternative quantity to recover is the 'far-field' data

$$\tilde{u}(x) := u(x, a)$$

for some $a > |g|_{L^\infty}$. We point out that there is some ambiguity in the term 'far-field' as some authors use this to characterize the propagating modes solely, whereas we use it to mean 'away' from the grating (where the evanescent modes will have exponentially small, but nonzero effect). As we comment later (section 3.3), the *location* of the far-field hyperplane $y = a$ has a strong influence on the behavior of our inversion algorithm. This value encodes the inherent ill-posedness of our recovery scheme and as a increases, the accuracy of our method deteriorates rather rapidly.

If we define the 'backward propagator' L by

$$L(g)[\tilde{u}(x)] := U(x),$$

then we can replace (3.2) with

$$(G - H)[L[\tilde{u}]] = \psi - H[\zeta], \tag{3.3}$$

or, for use with our inversion algorithms,

$$0 = Q(g)[\tilde{u}] := (G - H)[L[\tilde{u}]] - \psi + H[\zeta]. \tag{3.4}$$

3.1. A new algorithm for the forward problem

We propose a perturbative approach to the solution of (3.3) based upon the assumption $g(x) = \varepsilon f(x)$ where, *a priori*, ε is assumed small. If this is the case, then it can be shown that the data $\{\zeta, \psi\}$ and operators $\{G, H, L\}$ depend analytically upon ε so that

$$\zeta = \zeta(x;\varepsilon) = \sum_{n=0}^{\infty} \zeta_n(x)\varepsilon^n, \qquad \psi = \psi(x;\varepsilon) = \sum_{n=0}^{\infty} \psi_n(x)\varepsilon^n,$$

$$G = G(\varepsilon f) = \sum_{n=0}^{\infty} G_n(f)\varepsilon^n, \qquad H = H(\varepsilon f) = \sum_{n=0}^{\infty} H_n(f)\varepsilon^n,$$

$$L = L(\varepsilon f) = \sum_{n=0}^{\infty} L_n(f)\varepsilon^n,$$

and we assume

$$\tilde{u} = \tilde{u}(x;\varepsilon) = \sum_{n=0}^{\infty} \tilde{u}_n\varepsilon^n.$$

A rigorous justification for these expansions can be found in the work of Coifman and Meyer [CM85], Craig *et al* [CSS97], and the authors (in collaboration with Reitich and Hu) [NR01, NR03, NR04b, HN05, HN10]. Inserting this into (3.3), we see that

$$\left(\sum_{n=0}^{\infty} \varepsilon^n (G_n - H_n)\right)\left[\left(\sum_{s=0}^{\infty} \varepsilon^s L_s\right)\left[\sum_{m=0}^{\infty} \tilde{u}_m\varepsilon^m\right]\right] = \sum_{n=0}^{\infty} \psi_n\varepsilon^n - \left(\sum_{n=0}^{\infty} \varepsilon^n H_n\right)\left[\sum_{m=0}^{\infty} \zeta_m\varepsilon^m\right].$$

At order $\mathcal{O}(\varepsilon^0)$,

$$\tilde{u}_0 = L_0^{-1}[(G_0 - H_0)^{-1}[\psi_0 - H_0[\zeta_0]]], \tag{3.5}$$

while at order $\mathcal{O}(\varepsilon^n)$,

$$\sum_{s=0}^{n}\sum_{m=0}^{s}(G_{n-s} - H_{n-s})\,[L_{s-m}\,[\tilde{u}_m]] = \psi_n - \sum_{m=0}^{n} H_{n-m}\,[\zeta_m]\,.$$

Solving for $\tilde{u}_n$,

$$\tilde{u}_n = L_0^{-1}(G_0 - H_0)^{-1}\left\{\psi_n - \sum_{m=0}^{n} H_{n-m}\,[\zeta_m] - \sum_{s=0}^{n-1}\sum_{m=0}^{s}(G_{n-s} - H_{n-s})\,[L_{s-m}\,[\tilde{u}_m]]\right.$$
$$\left. - \sum_{m=0}^{n-1}(G_0 - H_0)\,[L_{n-m}\,[\tilde{u}_m]]\right\}. \tag{3.6}$$

Note that at *every* perturbation order in this approach, we repeatedly invert the common operator $(G_0 - H_0)L_0$ which is, in Fourier space, *diagonal* and can, therefore, be accomplished very rapidly.

3.2. Expansions: surface data

The key to both our forward and inverse algorithms are convenient, high order formulas for the functions ζ_n and ψ_n, and the operators G_n, H_n and L_n. We begin with ζ:

$$\zeta(x;\varepsilon) = -\mathrm{e}^{\mathrm{i}(\alpha x - \beta_u \varepsilon f(x))} = -\mathrm{e}^{\mathrm{i}\alpha x}\sum_{n=0}^{\infty} F_n(x)(-\mathrm{i}\beta_u)^n\varepsilon^n,$$

where $F_n(x) := f(x)^n/n!$. Thus,

$$\zeta_n = -\mathrm{e}^{\mathrm{i}\alpha x}F_n(x)(-\mathrm{i}\beta_u)^n. \tag{3.7}$$

Similarly, for ψ we have

$$\psi(x) = (\mathrm{i}\beta_u + \mathrm{i}\alpha\varepsilon(\partial_x f))\,\mathrm{e}^{\mathrm{i}(\alpha x - \beta_u\varepsilon f(x))}$$
$$= \mathrm{e}^{\mathrm{i}\alpha x}\left(\mathrm{i}\beta_u\sum_{n=0}^{\infty}F_n(x)(-\mathrm{i}\beta_u)^n\varepsilon^n + \mathrm{i}\alpha\varepsilon(\partial_x f)\sum_{n=0}^{\infty}F_n(x)(-\mathrm{i}\beta_u)^n\varepsilon^n\right).$$

So

$$\psi_n = \mathrm{e}^{\mathrm{i}\alpha x}(-F_n(x)(-\mathrm{i}\beta_u)^{n+1} + (\partial_x f)F_{n-1}(x)(\mathrm{i}\alpha)(-\mathrm{i}\beta_u)^{n-1}). \tag{3.8}$$

3.3. Expansions: backward propagator operator

The operators $\{L, G, H\}$ are a bit more involved and we will use the method of 'operator expansions' (OE) [Mil91a, CS93, NR04a] to find the action of $\{L_n, G_n, H_n\}$ on a Fourier basis function which, of course, leads to its action on any L^2 function. To begin, we consider the operator L which maps the far-field data $\tilde{u}$ to the surface data U. The function

$$u_p(x, y) = \mathrm{e}^{\mathrm{i}(\alpha_p x + \beta_{u,p}(y-a))}$$

satisfies Helmholtz's equation and the outgoing wave condition in the upper material. We can insert this into the definition of the operator L giving

$$L(g)[u_p(x, a)] = u_p(x, g(x))$$

or

$$L(g)[\mathrm{e}^{\mathrm{i}\alpha_p x}] = \mathrm{e}^{\mathrm{i}(\alpha_p x+\beta_{u,p}(g(x)-a))}.$$

Setting $g(x) = \varepsilon f(x)$, and expanding L and the exponential in the Taylor series reveals

$$\left(\sum_{n=0}^{\infty}\varepsilon^n L_n(f)\right)[\mathrm{e}^{\mathrm{i}\alpha_p x}] = \mathrm{e}^{\mathrm{i}\alpha_p x}\mathrm{e}^{-\mathrm{i}\beta_{u,p}a}\sum_{n=0}^{\infty}F_n(x)(\mathrm{i}\beta_{u,p})^n\varepsilon^n.$$

At order $\mathcal{O}(\varepsilon^0)$, we discover

$$L_0[\mathrm{e}^{\mathrm{i}\alpha_p x}] = \mathrm{e}^{-\mathrm{i}\beta_{u,p}a}\,\mathrm{e}^{\mathrm{i}\alpha_p x} = \mathrm{e}^{-\mathrm{i}\beta_{u,D}a}\,\mathrm{e}^{\mathrm{i}\alpha_p x},$$

where we have introduced a Fourier multiplier

$$m(D)[\xi(x)] := \sum_{p=-\infty}^{\infty} m(p)\hat{\xi}_p\,\mathrm{e}^{\mathrm{i}\alpha_p x}.$$

Using the fact that any α-quasiperiodic L^2 function can be expressed via its Fourier series, we deduce that

$$L_0[\xi] = \mathrm{e}^{-\mathrm{i}\beta_{u,D}a}\xi = \sum_{p=-\infty}^{\infty}\mathrm{e}^{-\mathrm{i}\beta_{u,p}a}\hat{\xi}_p\,\mathrm{e}^{\mathrm{i}\alpha_p x}.$$

At order $\mathcal{O}(\varepsilon^n)$ we find

$$L_n(f)[\mathrm{e}^{\mathrm{i}\alpha_p x}] = \mathrm{e}^{\mathrm{i}\alpha_p x}\mathrm{e}^{-\mathrm{i}\beta_{u,p}a}F_n(x)(\mathrm{i}\beta_{u,p})^n = F_n(x)\,\mathrm{e}^{-\mathrm{i}\beta_{u,D}a}(\mathrm{i}\beta_{u,D})^n\,\mathrm{e}^{\mathrm{i}\alpha_p x},$$

so that

$$L_n(f)[\xi] = F_n(x)\,\mathrm{e}^{-\mathrm{i}\beta_{u,D}a}(\mathrm{i}\beta_{u,D})^n\xi = F_n(x)L_0(\mathrm{i}\beta_{u,D})^n\xi = F_n(x)(\mathrm{i}\beta_{u,D})^n L_0\xi. \tag{3.9}$$

Remark. We will soon introduce an inversion algorithm for the interface shape g based upon the formulas presented in these sections. A fundamental feature of such problems is severe ill-posedness and we point out that this is reflected in the operator L_0. For p corresponding to propagating waves (p sufficiently small), we have chosen $\beta_{u,p}$ real so that the Fourier multiplier $\exp(-\mathrm{i}\beta_{u,p}a)$ is of modulus one. However, for p corresponding to evanescent modes (p large), $\beta_{u,p}$ is purely imaginary with a positive imaginary part, cf (2.4). Therefore, while the operator L_0^{-1}, which factors into the forward solve (see (3.5)), is exponentially smoothing, the operator L_0 *amplifies* Fourier coefficients of large index exponentially.

3.4. Expansions: Dirichlet–Neumann operators

Consider now the DNO G which maps the surface Dirichlet data U to the surface normal derivative U'. We now (slightly) redefine the function

$$u_p(x, y) = \mathrm{e}^{\mathrm{i}(\alpha_p x+\beta_{u,p}y)}$$

which again satisfies Helmholtz's equation and the outgoing wave condition in the upper material. We can insert this into the definition of the operator G giving

$$G(g)\left[u_p(x, g(x))\right] = (\partial_y u_p)(x, g(x)) - (\partial_x g)(\partial_x u_p)(x, g(x)),$$

or

$$G(g)\left[\mathrm{e}^{\mathrm{i}(\alpha_p x+\beta_{u,p}g(x))}\right] = \left(\mathrm{i}\beta_{u,p} - (\partial_x g)\mathrm{i}\alpha_p\right)\mathrm{e}^{\mathrm{i}(\alpha_p x+\beta_{u,p}g(x))}.$$

Again setting $g(x) = \varepsilon f(x)$, and expanding G and the exponentials in the Taylor series gives

$$\left(\sum_{n=0}^{\infty}\varepsilon^n G_n(f)\right)\left[\mathrm{e}^{\mathrm{i}\alpha_p x}\sum_{m=0}^{\infty}F_m(x)(\mathrm{i}\beta_{u,p})^m\varepsilon^m\right] = \mathrm{i}\beta_{u,p}\,\mathrm{e}^{\mathrm{i}\alpha_p x}\sum_{n=0}^{\infty}F_n(x)(\mathrm{i}\beta_{u,p})^n\varepsilon^n$$
$$-\varepsilon(\partial_x f)(\mathrm{i}\alpha_p)\,\mathrm{e}^{\mathrm{i}\alpha_p x}\sum_{n=0}^{\infty}F_n(x)(\mathrm{i}\beta_{u,p})^n\varepsilon^n.$$

At order $\mathcal{O}(\varepsilon^0)$, we find

$$G_0[\mathrm{e}^{\mathrm{i}\alpha_p x}] = (\mathrm{i}\beta_{u,p})\,\mathrm{e}^{\mathrm{i}\alpha_p x} = (\mathrm{i}\beta_{u,D})\,\mathrm{e}^{\mathrm{i}\alpha_p x}$$

or

$$G_0[\xi] = (\mathrm{i}\beta_{u,D})\xi.$$

At order $\mathcal{O}(\varepsilon^n)$, we obtain

$$\sum_{m=0}^{n}G_m[F_{n-m}(\mathrm{i}\beta_{u,p})^{n-m}\,\mathrm{e}^{\mathrm{i}\alpha_p x}] = F_n(x)(\mathrm{i}\beta_{u,p})^{n+1}\,\mathrm{e}^{\mathrm{i}\alpha_p x} - (\partial_x f)F_{n-1}(x)(\mathrm{i}\alpha_p)(\mathrm{i}\beta_{u,p})^{n-1}\,\mathrm{e}^{\mathrm{i}\alpha_p x}$$

or

$$G_n[\mathrm{e}^{\mathrm{i}\alpha_p x}] = \{F_n(x)(\mathrm{i}\beta_{u,p})^2 - (\partial_x f)F_{n-1}(x)(\mathrm{i}\alpha_p)\}(\mathrm{i}\beta_{u,p})^{n-1}\,\mathrm{e}^{\mathrm{i}\alpha_p x}$$
$$-\sum_{m=0}^{n-1}G_m[F_{n-m}(\mathrm{i}\beta_{u,p})^{n-m}\,\mathrm{e}^{\mathrm{i}\alpha_p x}].$$

Since

$$\alpha_p^2 + \beta_{u,p}^2 = k_u^2$$

we have

$$(\mathrm{i}\alpha_p)^2 + (\mathrm{i}\beta_{u,p})^2 = -k_u^2$$

and

$$(\mathrm{i}\beta_{u,p})^2 = -k_u^2 - (\mathrm{i}\alpha_p)^2.$$

Thus,

$$\begin{aligned}G_n[\mathrm{e}^{\mathrm{i}\alpha_p x}] &= \left\{-k_u^2F_n(x) - F_n(x)(\mathrm{i}\alpha_p)^2 - (\partial_x f)F_{n-1}(x)(\mathrm{i}\alpha_p)\right\}(\mathrm{i}\beta_{u,p})^{n-1}\,\mathrm{e}^{\mathrm{i}\alpha_p x}\\ &\quad -\sum_{m=0}^{n-1}G_m[F_{n-m}(\mathrm{i}\beta_{u,p})^{n-m}\,\mathrm{e}^{\mathrm{i}\alpha_p x}]\\ &= -k_u^2F_n(x)(\mathrm{i}\beta_{u,D})^{n-1}\,\mathrm{e}^{\mathrm{i}\alpha_p x} - \partial_x[F_n(x)\partial_x(\mathrm{i}\beta_{u,D})^{n-1}\,\mathrm{e}^{\mathrm{i}\alpha_p x}]\\ &\quad -\sum_{m=0}^{n-1}G_m[F_{n-m}(\mathrm{i}\beta_{u,D})^{n-m}\,\mathrm{e}^{\mathrm{i}\alpha_p x}],\end{aligned}$$

where we have used

$$\partial_x\,\mathrm{e}^{\mathrm{i}\alpha_p x} = (\mathrm{i}\alpha_p)\,\mathrm{e}^{\mathrm{i}\alpha_p x}.$$

Finally,

$$G_n[\xi] = -k_u^2F_n(x)(\mathrm{i}\beta_{u,D})^{n-1}\xi - \partial_x[F_n(x)\partial_x(\mathrm{i}\beta_{u,D})^{n-1}\xi] - \sum_{m=0}^{n-1}G_m[F_{n-m}(\mathrm{i}\beta_{u,D})^{n-m}\xi]. \tag{3.10}$$

In particular, for use in section 4.1,

$$\begin{aligned} G_1[\xi] &= -k_u^2 f\xi - \partial_x[f\partial_x\xi] - G_0[f(\mathrm{i}\beta_{u,D})\xi] \\ &= -k_u^2 f\xi - \partial_x[f\partial_x\xi] - G_0[fG_0\xi]. \end{aligned}$$

In an exactly analogous fashion, consider the DNO H which maps the surface Dirichlet data V to the surface normal derivative V'. Specify the function

$$v_p(x, y) = \mathrm{e}^{\mathrm{i}(\alpha_p x - \beta_{v,p} y)}$$

which satisfies Helmholtz's equation and the outgoing wave condition in the lower material. We can insert this into the definition of the operator H giving

$$H(g)[v_p(x, g(x))] = (\partial_y v_p)(x, g(x)) - (\partial_x g)(\partial_x v_p)(x, g(x))$$

or

$$H(g)[\mathrm{e}^{\mathrm{i}(\alpha_p x - \beta_{v,p} g(x))}] = (-\mathrm{i}\beta_{v,p} - (\partial_x g)\mathrm{i}\alpha_p)\,\mathrm{e}^{\mathrm{i}(\alpha_p x - \beta_{v,p} g(x))}.$$

Once again setting $g(x) = \varepsilon f(x)$, and expanding H and the exponentials in the Taylor series gives

$$\begin{aligned} \left(\sum_{n=0}^{\infty} \varepsilon^n H_n(f)\right)\left[\mathrm{e}^{\mathrm{i}\alpha_p x}\sum_{m=0}^{\infty} F_m(x)(-\mathrm{i}\beta_{v,p})^m\varepsilon^m\right] &= -\mathrm{i}\beta_{v,p}\,\mathrm{e}^{\mathrm{i}\alpha_p x}\sum_{n=0}^{\infty} F_n(x)(-\mathrm{i}\beta_{v,p})^n\varepsilon^n \\ &\quad - \varepsilon(\partial_x f)(\mathrm{i}\alpha_p)\,\mathrm{e}^{\mathrm{i}\alpha_p x}\sum_{n=0}^{\infty} F_n(x)(-\mathrm{i}\beta_{v,p})^n\varepsilon^n. \end{aligned}$$

At order $\mathcal{O}(\varepsilon^0)$ we find

$$H_0[\mathrm{e}^{\mathrm{i}\alpha_p x}] = -(\mathrm{i}\beta_{v,p})\,\mathrm{e}^{\mathrm{i}\alpha_p x} = -(\mathrm{i}\beta_{v,D})\,\mathrm{e}^{\mathrm{i}\alpha_p x}$$

or

$$H_0[\xi] = -(\mathrm{i}\beta_{v,D})\xi.$$

At order $\mathcal{O}(\varepsilon^n)$, we obtain

$$\begin{aligned} \sum_{m=0}^{n} H_m[F_{n-m}(-\mathrm{i}\beta_{v,p})^{n-m}\,\mathrm{e}^{\mathrm{i}\alpha_p x}] &= F_n(x)(-\mathrm{i}\beta_{v,p})^{n+1}\,\mathrm{e}^{\mathrm{i}\alpha_p x} \\ &\quad - (\partial_x f)F_{n-1}(x)(\mathrm{i}\alpha_p)(-\mathrm{i}\beta_{v,p})^{n-1}\,\mathrm{e}^{\mathrm{i}\alpha_p x} \end{aligned}$$

or

$$\begin{aligned} H_n[\mathrm{e}^{\mathrm{i}\alpha_p x}] &= \{F_n(x)(-\mathrm{i}\beta_{v,p})^2 - (\partial_x f)F_{n-1}(x)(\mathrm{i}\alpha_p)\}(-\mathrm{i}\beta_{v,p})^{n-1}\,\mathrm{e}^{\mathrm{i}\alpha_p x} \\ &\quad - \sum_{m=0}^{n-1} H_m[F_{n-m}(-\mathrm{i}\beta_{v,p})^{n-m}\,\mathrm{e}^{\mathrm{i}\alpha_p x}]. \end{aligned}$$

As before

$$(-\mathrm{i}\beta_{v,p})^2 = -k_v^2 - (-\mathrm{i}\alpha_p)^2 = -k_v^2 - (\mathrm{i}\alpha_p)^2.$$

Thus,

$$\begin{aligned} H_n[\mathrm{e}^{\mathrm{i}\alpha_p x}] &= \left\{-k_v^2 F_n(x) - F_n(x)(\mathrm{i}\alpha_p)^2 - (\partial_x f)F_{n-1}(x)(\mathrm{i}\alpha_p)\right\}(-\mathrm{i}\beta_{v,p})^{n-1}\,\mathrm{e}^{\mathrm{i}\alpha_p x} \\ &\quad - \sum_{m=0}^{n-1} H_m[F_{n-m}(-\mathrm{i}\beta_{v,p})^{n-m}\,\mathrm{e}^{\mathrm{i}\alpha_p x}] \\ &= -k_v^2 F_n(x)(-\mathrm{i}\beta_{v,D})^{n-1}\,\mathrm{e}^{\mathrm{i}\alpha_p x} - \partial_x[F_n(x)\partial_x(-\mathrm{i}\beta_{v,D})^{n-1}\,\mathrm{e}^{\mathrm{i}\alpha_p x}] \\ &\quad - \sum_{m=0}^{n-1} H_m[F_{n-m}(-\mathrm{i}\beta_{v,D})^{n-m}\,\mathrm{e}^{\mathrm{i}\alpha_p x}]. \end{aligned}$$

Finally,

$$H_n[\xi] = -k_v^2 F_n(x)(-\mathrm{i}\beta_{v,D})^{n-1}\xi - \partial_x[F_n(x)\partial_x(-\mathrm{i}\beta_{v,D})^{n-1}\xi] - \sum_{m=0}^{n-1} H_m[F_{n-m}(-\mathrm{i}\beta_{v,D})^{n-m}\xi]. \tag{3.11}$$

In particular, again for the use in section 4.1,

$$\begin{aligned} H_1[\xi] &= -k_v^2 f\xi - \partial_x[f\partial_x\xi] - H_0[f(-\mathrm{i}\beta_{v,D})\xi] \\ &= -k_v^2 f\xi - \partial_x[f\partial_x\xi] - H_0[fH_0\xi]. \end{aligned}$$

3.5. Forward solve: flat interface

With formulas for the operators now in place we can utilize formulas (3.5) and (3.6) to find approximations to the $\tilde{u}_n$ and form

$$\tilde{u}^N(x;\varepsilon) := \sum_{n=0}^{N} \tilde{u}_n(x)\varepsilon^n. \tag{3.12}$$

Before beginning we point out that the relevant Fourier multipliers (e.g. $\mathrm{i}\beta_{v,D}$) have a particularly simple action on the single mode $\mathrm{e}^{\mathrm{i}\alpha x}$. For example, since

$$\mathrm{e}^{\mathrm{i}\alpha x} = \sum_{p=-\infty}^{\infty} d_p\,\mathrm{e}^{\mathrm{i}\alpha_p x}, \qquad d_p = \begin{cases} 1 & p = 0 \\ 0 & p \neq 0 \end{cases},$$

we have

$$\mathrm{i}\beta_{v,D}[\mathrm{e}^{\mathrm{i}\alpha x}] = \mathrm{i}\beta_{v,D}\left[\sum_{p=-\infty}^{\infty} d_p\,\mathrm{e}^{\mathrm{i}\alpha_p x}\right] = \sum_{p=-\infty}^{\infty} (\mathrm{i}\beta_{v,p})d_p\,\mathrm{e}^{\mathrm{i}\alpha_p x} = \mathrm{i}\beta_v\,\mathrm{e}^{\mathrm{i}\alpha x}.$$

Returning to our solution algorithm, (3.5) can now be written as

$$\begin{aligned} \tilde{u}_0 &= \mathrm{e}^{\mathrm{i}\beta_{u,D}a}[(\mathrm{i}\beta_{u,D} + \mathrm{i}\beta_{v,D})^{-1}[(\mathrm{i}\beta_u)\,\mathrm{e}^{\mathrm{i}\alpha x} + \mathrm{i}\beta_{v,D}[-\mathrm{e}^{\mathrm{i}\alpha x}]] \\ &= \mathrm{e}^{\mathrm{i}\beta_{u,D}a}[(\mathrm{i}\beta_{u,D} + \mathrm{i}\beta_{v,D})^{-1}[(\mathrm{i}\beta_u - \mathrm{i}\beta_v)]\,\mathrm{e}^{\mathrm{i}\alpha x}] \\ &= \mathrm{e}^{\mathrm{i}\beta_{u,D}a}\left[\frac{(\mathrm{i}\beta_u - \mathrm{i}\beta_v)}{(\mathrm{i}\beta_u + \mathrm{i}\beta_v)}\,\mathrm{e}^{\mathrm{i}\alpha x}\right] \\ &= \mathrm{e}^{\mathrm{i}\beta_u a}\frac{(\mathrm{i}\beta_u - \mathrm{i}\beta_v)}{(\mathrm{i}\beta_u + \mathrm{i}\beta_v)}\,\mathrm{e}^{\mathrm{i}\alpha x}, \end{aligned} \tag{3.13}$$

which is, of course, the *exact* solution in the flat interface ($\varepsilon = 0$) case and recovers the plane-wave reflection coefficients.

Remark. We note that in this simple flat-interface case

$$\psi_0 = G_0[\zeta_0]$$

so that (3.5) simplifies to

$$\tilde{u}_0 = L_0^{-1}[(G_0 - H_0)^{-1}[(G_0 - H_0)[\zeta_0]]] = L_0^{-1}[\zeta_0]$$

as expected.

Remark. We point out here that this formula can also be used as a very primitive inverse problem solver. If we specify the incident radiation (in particular β_u) and measure the far-field pattern $\tilde{u}_0$ at the known plane $y = a$, then (3.13) can be solved for β_v which gives very rough

Table 1. Absolute and relative L^∞ errors in approximation of the far-field pattern $\tilde{u}$ at $a = 1$. Physical parameters: $\alpha = 0.1$, $\beta_u = 1.1$, $\beta_v = 5.5$, $d = 2\pi$, $a = 1$; numerical parameter: $N_x = 32$.

N	Absolute L^∞ error	Relative L^∞ error
0	0.000 196 114	0.000 294 154
1	$4.518\,06 \times 10^{-8}$	$6.776\,71 \times 10^{-8}$
2	$3.228\,02 \times 10^{-10}$	$4.841\,76 \times 10^{-10}$
3	$3.282\,69 \times 10^{-10}$	$4.923\,77 \times 10^{-10}$
4	3.2827×10^{-10}	$4.923\,77 \times 10^{-10}$

material properties of the lower layer. Note that (3.13) demands that $\tilde{u}_0$ have the rather trivial Fourier series

$$\tilde{u}_0(x) = \tilde{u}_{0,0}\, e^{i\alpha},$$

but, given this, one can use (3.13) to deduce that

$$\beta_v = \beta_u \left(\frac{e^{i\beta_u a} - \tilde{u}_{0,0}}{e^{i\beta_u a} + \tilde{u}_{0,0}} \right). \tag{3.14}$$

3.6. Numerical results for a general interface

To briefly test this new algorithm for the forward problem we select a configuration with physical parameters

$$\alpha = 0.1, \qquad \beta_u = 1.1, \qquad \beta_v = 5.5,$$

cf (2.2*f*) and (2.2*g*) with a $d = 2\pi$-periodic layer interface shaped by

$$g(x) = \varepsilon f(x) = \varepsilon\, e^{\cos(2x)},$$

and 'far-field' $\tilde{u}$ at $a = 1$. To compute an 'exact solution', we utilize the method of field expansions (FE) [BR93a] as implemented by the authors in the recent publication [MN11]. While the methods are related (both are spectral collocation boundary perturbation approaches), they are *not* identical and one provides an excellent test for the other. For the configuration mentioned above and $\varepsilon = 0.0001$, we performed a numerical simulation using the FE approach with $N_x = 128$ collocation points and $N = 40$ Taylor orders (Taylor summation was used); please see [MN11] for more details regarding the algorithm and these parameters.

In table 1, we present results of a numerical implementation of (3.5) and (3.6) to deliver (3.12), reporting perturbation order versus absolute and relative errors. Here we note the very stable and rapid (exponential) convergence of our numerical approximation to the 'exact solution' provided by the FE method.

4. Inverse problem

Our real goal in this paper is to devise a technique for recovering the layer interface, $g(x)$, from surface measurements. In this initial contribution, we propose as given data the incident radiation:

$$u^i(x, y) = e^{i\alpha x - i\beta_u y}$$

(which includes the material properties of the upper layer through β_u) the 'far-field pattern' $\tilde{u}(x)$ at *all* values of x, and the most basic material properties of the lower layer β_v (which we assume can be recovered from (3.14) or some other method).

4.1. Iteration-free linear model

With these constraints in mind, consider the forward problem (3.4) and suppose that the unknown interface can be expressed as $g(x) = \varepsilon f(x)$. In this case, we have

$$(G_0 + \varepsilon G_1 - H_0 - \varepsilon H_1)[(L_0 + \varepsilon L_1)[\tilde{u}]] - \psi_0 - \varepsilon\psi_1 + (H_0 + \varepsilon H_1)[\zeta_0 + \varepsilon\zeta_1] = \mathcal{O}(\varepsilon^2).$$

More precisely, and making the f dependence explicit, we have

$$\begin{aligned}(G_0 - H_0)L_0[\tilde{u}] + \varepsilon(G_0 - H_0)L_1(f)[\tilde{u}] + \varepsilon(G_1(f) - H_1(f))L_0[\tilde{u}] \\ - \psi_0 - \varepsilon\psi_1(f) + H_0[\zeta_0] + \varepsilon H_1(f)[\zeta_0] + \varepsilon H_0[\zeta_1(f)] = \mathcal{O}(\varepsilon^2).\end{aligned}$$

For a first algorithm, we ignore the $\mathcal{O}(\varepsilon^2)$ terms and gather the $\mathcal{O}(1)$ and $\mathcal{O}(\varepsilon)$ terms separately:

$$Q_0(\tilde{u}) + \varepsilon Q_1(\tilde{u})[f] = 0, \tag{4.1a}$$

where

$$Q_0(\tilde{u}) := (G_0 - H_0)L_0[\tilde{u}] - \psi_0 + H_0[\zeta_0] \tag{4.1b}$$

$$\begin{aligned}Q_1(\tilde{u})[f] := (G_0 - H_0)L_1(f)[\tilde{u}] + (G_1(f) - H_1(f))L_0[\tilde{u}] - \psi_1(f) \\ + H_1(f)[\zeta_0] + H_0[\zeta_1(f)].\end{aligned} \tag{4.1c}$$

The operator $Q_1(\cdot)[\tilde{u}]$ is linear in f, though in a rather implicit way, and we propose the following solution formula:

$$\tilde{g} = -\{Q_1(\cdot)[\tilde{u}]\}^{-1} Q_0[\tilde{u}], \tag{4.2}$$

where $\tilde{g} \approx g$. Note that this approach is 'linear' (i.e. terms of order 2 and higher were ignored) and the unique solution can be found rather directly (without iteration) by simply inverting the linear operator (represented as a matrix in a numerical simulation), $Q_1(\cdot)(\tilde{u})$.

Remark. As we mentioned earlier (section 3.3), the operators L_0 and $L_1 = f(\mathrm{i}\beta_{u,D})L_0$, (3.9), are ill-conditioned resulting in potentially unstable numerics. However, such ill-conditioning is a standard feature of inverse problems [CK98] and it is to be expected in such algorithms.

4.2. Iterative nonlinear model

To devise a second, and hopefully more accurate approach, we return to the forward problem (3.4) and again suppose that the unknown interface can be expressed as $g(x) = \varepsilon f(x)$. Now,

$$Q_0(\tilde{u}) + \varepsilon Q_1(\tilde{u})[f] + \sum_{n=2}^{N} \varepsilon^n Q_n(\tilde{u}, f) = \mathcal{O}(\varepsilon^{N+1}), \tag{4.3}$$

where

$$Q_n(\tilde{u}, f) = \sum_{m=0}^{n} (G_{n-m}(f) - H_{n-m}(f))\,[L_m(f)\,[\tilde{u}]] - \psi_n(f) + \sum_{m=0}^{n} H_{n-m}(f)\,[\zeta_m(f)]\,.$$

A natural algorithm which suggests itself is to combine the higher accuracy of the expansion (4.3) for $N > 1$ with the ease of inversion of (4.2); thus, we drop the $\mathcal{O}(\varepsilon^{N+1})$ term in (4.3), mark the linear (in ε) term with iteration number $k + 1$, and all other terms with iteration number k resulting in the Picard iteration [BF97, AH01]

$$\tilde{g}^{k+1} = -\{Q_1(\cdot)[\tilde{u}]\}^{-1} \left[Q_0[\tilde{u}] + \sum_{n=2}^{N} Q_n(\tilde{u}, \tilde{g}^k) \right]. \tag{4.4}$$

Table 2. Absolute and relative L^∞ errors in approximation of the analytic profile $y = \varepsilon\, e^{\cos(2x)}$, (4.5), using the exact linear model, (4.2), for reconstruction. Physical parameters: $\alpha = 0$, $\beta_u = 1.1$, $\beta_v = 5.5$, $d = 2\pi$, $a = 1$; numerical parameters: $N_x = 32$, $N_{\text{forward}} = 10$.

ε	Absolute L^∞ error	Relative L^∞ error
0.001	$3.403\,41 \times 10^{-6}$	0.001 252 05
0.002	$1.354\,04 \times 10^{-5}$	0.002 490 62
0.003	$3.029\,75 \times 10^{-5}$	0.003 715 28
0.004	$5.357\,26 \times 10^{-5}$	0.004 927 06
0.005	$8.326\,29 \times 10^{-5}$	0.006 126 14
0.006	0.000 119 28	0.007 313 42
0.007	0.000 161 528	0.008 489
0.008	0.000 209 926	0.009 653 43
0.009	0.000 264 389	0.010 807
0.01	0.000 324 838	0.011 9501

Table 3. Absolute and relative L^∞ errors in approximation of the analytic profile $y = \varepsilon\, e^{\cos(2x)}$, (4.5), using the nonlinear model, (4.4), for reconstruction. Physical parameters: $\alpha = 0$, $\beta_u = 1.1$, $\beta_v = 5.5$, $d = 2\pi$, $a = 1$; numerical parameters: $N_x = 32$, $N_{\text{forward}} = 10$, $\tau = 10^{-8}$, $N_{\text{inverse}} = 4$.

ε	Number of iterations	Absolute L^∞ error	Relative L^∞ error
0.001	4	$1.219\,23 \times 10^{-9}$	$4.485\,31 \times 10^{-7}$
0.002	5	$1.053\,61 \times 10^{-9}$	1.938×10^{-7}
0.003	6	$1.506\,81 \times 10^{-9}$	$1.847\,75 \times 10^{-7}$
0.004	7	$3.999\,85 \times 10^{-9}$	$3.678\,65 \times 10^{-7}$
0.005	8	$7.419\,19 \times 10^{-9}$	$5.458\,73 \times 10^{-7}$
0.006	9	$2.035\,56 \times 10^{-8}$	$1.248\,07 \times 10^{-6}$
0.007	10	$4.269\,12 \times 10^{-8}$	2.2436×10^{-6}
0.008	11	$8.298\,94 \times 10^{-8}$	$3.816\,26 \times 10^{-6}$
0.009	12	$1.501\,13 \times 10^{-7}$	$6.135\,94 \times 10^{-6}$
0.01	13	$2.565\,47 \times 10^{-7}$	$9.437\,82 \times 10^{-6}$

Note that in the case $N = 1$, this becomes our linear algorithm (4.2). However, in contrast with (4.2), this new method is 'nonlinear' (as we now retain quadratic and higher terms) and requires an iteration scheme for its solution. As with any iterative scheme it is of paramount importance to select a good initial guess. For this, we recommend using the linear approximation (4.2)

$$\tilde{g}^0 = -\{Q_1(\cdot)[\tilde{u}]\}^{-1}\, Q_0[\tilde{u}].$$

4.3. Results

We now demonstrate the capabilities of our new algorithms with a sequence of numerical studies. To begin, we consider the analytic and $d = 2\pi$-periodic profile

$$g(x) = \varepsilon\, e^{\cos(2x)} \tag{4.5}$$

(see figure 1) as the shape of the interface between two materials with $k_u = 1.1$ and $k_v = 5.5$. Utilizing our algorithm for the forward problem, (3.6), we generate a far-field pattern $\tilde{u}$ (with

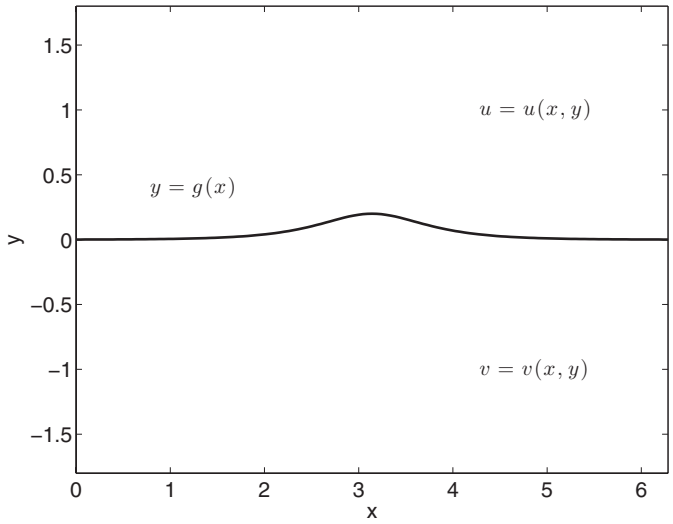

Figure 2. Problem configuration with layer boundary (solid line); here $g(x) = 0.2\text{sech}(2(x - \pi))$.

Table 4. Absolute and relative L^∞ errors in approximation of the Gaussian profile $y = \varepsilon\,\text{sech}(bx)$ ($b = 2$), (4.6), using the exact linear model, (4.2), for reconstruction. Physical parameters: $\alpha = 0.2$, $\beta_u = 1.3$, $\beta_v = 6.8$, $d = 2\pi$, $a = 1$; numerical parameters: $N_x = 32$, $N_{\text{forward}} = 10$.

ε	Absolute L^∞ error	Relative L^∞ error
0.001	$3.592\,24 \times 10^{-7}$	0.000 359 224
0.002	$1.434\,28 \times 10^{-6}$	0.000 717 14
0.003	$3.221\,59 \times 10^{-6}$	0.001 073 86
0.004	$5.717\,94 \times 10^{-6}$	0.001 429 49
0.005	$8.921\,24 \times 10^{-6}$	0.001 784 25
0.006	$1.282\,65 \times 10^{-5}$	0.002 137 76
0.007	$1.743\,17 \times 10^{-5}$	0.002 490 24
0.008	2.2733×10^{-5}	0.002 841 63
0.009	$2.872\,92 \times 10^{-5}$	0.003 192 13
0.01	$3.541\,61 \times 10^{-5}$	0.003 541 61

$N_x = 32$ equally spaced grid points and $N = N_{\text{forward}} = 10$ Taylor orders). Using the 'linear model' (4.2), we produce the approximation $\tilde{g}_0$ and in table 2 report on the absolute and relative supremum norm errors in the recovery of g for various values of ε. We note the rapid rate of convergence as $\varepsilon \to 0$ which is repeated for all of the profiles considered here. Additionally, we use the nonlinear iterative approach (4.4) to approximate g (with initial guess $\tilde{g}_0$, $N = N_{\text{inverse}} = 4$, and tolerance $\tau = 10^{-8}$ for the iteration) and display these absolute and relative errors in table 3. In these, we see not only the rapid and stable convergence of both of our new approaches to the specified boundary shape $g(x)$ but also the highly advantageous nature of the nonlinear iteration scheme which can generate three to four more digits of accuracy with only a modest (4–13) number of iterations.

We now move on to two other profiles, one meant to resemble a Gaussian pulse

$$g_G(x) = \varepsilon\,\text{sech}(b(x - d/2)) \tag{4.6}$$

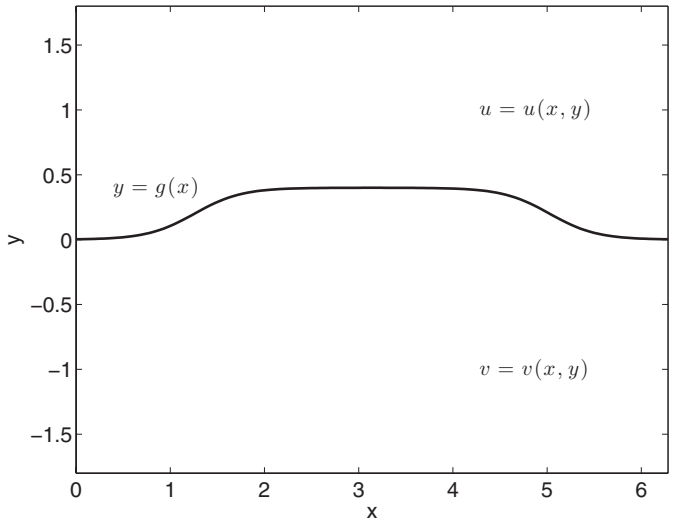

Figure 3. Problem configuration with layer boundary (solid line); here $g(x) = 0.2\,[\tanh(2((x-\pi)+3\pi/5)) - \tanh(2(x-\pi)-3\pi/5))]$.

Table 5. Absolute and relative L^∞ errors in approximation of the Gaussian profile $y = \varepsilon\,\mathrm{sech}(bx)$ ($b = 2$), (4.6), using the nonlinear model, (4.4), for reconstruction. Physical parameters: $\alpha = 0.2$, $\beta_u = 1.3$, $\beta_v = 6.8$, $d = 2\pi$, $a = 1$; numerical parameters: $N_x = 32$, $N_{\text{forward}} = 10$, $\tau = 10^{-8}$, $N_{\text{inverse}} = 4$.

ε	Number of iterations	Absolute L^∞ error	Relative L^∞ error
0.001	3	$5.693\,07 \times 10^{-10}$	$5.693\,07 \times 10^{-7}$
0.002	4	$5.209\,79 \times 10^{-10}$	2.6049×10^{-7}
0.003	4	5.9729×10^{-10}	$1.990\,97 \times 10^{-7}$
0.004	5	$4.019\,66 \times 10^{-10}$	$1.004\,92 \times 10^{-7}$
0.005	5	$8.179\,42 \times 10^{-10}$	$1.635\,88 \times 10^{-7}$
0.006	5	$6.833\,63 \times 10^{-10}$	$1.138\,94 \times 10^{-7}$
0.007	6	$6.816\,67 \times 10^{-10}$	$9.738\,11 \times 10^{-8}$
0.008	6	$5.429\,17 \times 10^{-10}$	$6.786\,46 \times 10^{-8}$
0.009	6	$1.056\,07 \times 10^{-9}$	$1.173\,41 \times 10^{-7}$
0.01	7	$2.168\,23 \times 10^{-9}$	$2.168\,23 \times 10^{-7}$

and another meant to model a smoothed bar

$$g_B(x) = \varepsilon\,[\tanh(b((x - d/2) + c)) - \tanh(b(x - (d/2) - c))]\,; \tag{4.7}$$

see figures 2 and 3.

For these interfaces, we select $\alpha = 0.2$ and materials such that $\beta_u = 1.3$ and $\beta_v = 6.8$ (so that $k_u \approx 1.3153$ and $k_v \approx 6.8029$). Once again we produce a far-field pattern using our forward algorithm, (3.6), with $N_x = 32$ equally spaced grid points and $N_{\text{forward}} = 10$ Taylor orders. With the 'linear model' (4.2) we produce the approximation $\tilde{g}_0$ and in tables 4 and 6 report on the absolute and relative supremum norm errors in the recovery of g_G and g_B, respectively. Additionally, we use the nonlinear iterative approach (4.4) to approximate g_G and g_B (with initial guess $\tilde{g}_0$, degree of nonlinearity $N_{\text{inverse}} = 4$ and tolerance $\tau = 10^{-8}$) and display these absolute and relative errors in tables 5 and 7. As with the analytic profile above,

Table 6. Absolute and relative L^∞ errors in approximation of the bar profile $y = \varepsilon\,[\tanh(b(x+c)) - \tanh(b(x-c))]$ ($b = 2$, $c = 3\pi/5$), (4.7), using the exact linear model, (4.2), for reconstruction. Physical parameters: $\alpha = 0.2$, $\beta_u = 1.3$, $\beta_v = 6.8$, $d = 2\pi$, $a = 1$; numerical parameters: $N_x = 32$, $N_{\text{forward}} = 10$.

ε	Absolute L^∞ error	Relative L^∞ error
0.001	$4.440\,73 \times 10^{-7}$	0.000 222 273
0.002	$1.778\,19 \times 10^{-6}$	0.000 445 019
0.003	$4.003\,01 \times 10^{-6}$	0.000 667 879
0.004	$7.121\,05 \times 10^{-6}$	0.000 891 079
0.005	$1.113\,26 \times 10^{-5}$	0.001 114 45
0.006	$1.603\,95 \times 10^{-5}$	0.001 338 05
0.007	$2.184\,09 \times 10^{-5}$	0.001 561 72
0.008	$2.853\,84 \times 10^{-5}$	0.001 785 55
0.009	$3.613\,23 \times 10^{-5}$	0.002 009 49
0.01	$4.462\,44 \times 10^{-5}$	0.002 233 59

Table 7. Absolute and relative L^∞ errors in the approximation of the bar profile $y = \varepsilon\,[\tanh(b(x+c)) - \tanh(b(x-c))]$ ($b = 2$, $c = 3\pi/5$), (4.7), using the nonlinear model, (4.4), for reconstruction. Physical parameters: $\alpha = 0.2$, $\beta_u = 1.3$, $\beta_v = 6.8$, $d = 2\pi$, $a = 1$; numerical parameters: $N_x = 32$, $N_{\text{forward}} = 10$, $\tau = 10^{-8}$, $N_{\text{inverse}} = 4$.

ε	Number of iterations	Absolute L^∞ error	Relative L^∞ error
0.001	3	$4.145\,24 \times 10^{-10}$	$2.074\,82 \times 10^{-7}$
0.002	4	$2.980\,51 \times 10^{-10}$	7.4592×10^{-8}
0.003	5	$7.764\,37 \times 10^{-10}$	$1.295\,44 \times 10^{-7}$
0.004	5	$8.704\,47 \times 10^{-10}$	$1.089\,22 \times 10^{-7}$
0.005	5	$8.920\,73 \times 10^{-10}$	$8.930\,22 \times 10^{-8}$
0.006	6	$9.983\,51 \times 10^{-10}$	$8.328\,44 \times 10^{-8}$
0.007	6	$1.935\,22 \times 10^{-9}$	$1.383\,77 \times 10^{-7}$
0.008	6	$3.512\,24 \times 10^{-9}$	$2.197\,49 \times 10^{-7}$
0.009	7	$6.066\,07 \times 10^{-9}$	$3.373\,62 \times 10^{-7}$
0.01	7	$1.012\,94 \times 10^{-8}$	$5.070\,09 \times 10^{-7}$

we note both the rapid convergence of our approach, and the truly superior accuracy one can achieve with the nonlinear iterative methodology.

Acknowledgments

DPN gratefully acknowledges support from the National Science Foundation through grant no DMS-0810958 and the Department of Energy under award no DE-SC0001549. AM thanks the Earth Resources Laboratory Founding Members Consortium for support.

Disclaimer

product, or process disclosed, or represents that its use would not infringe privately owned rights. Reference herein to any specific commercial product, process, or service by trade name, trademark, manufacturer, or otherwise does not necessarily constitute or imply its endorsement, recommendation, or favoring by the United States Government or any agency thereof. The views and opinions of authors expressed herein do not necessarily state or reflect those of the United States Government or any agency thereof.

References

[AH01] Atkinson K and Han W 2001 A functional analysis framework *Theoretical Numerical Analysis* (*Texts in Applied Mathematics* vol 39) (New York: Springer)

[AKY06] Akduman I, Kress R and Yapar A 2006 Iterative reconstruction of dielectric rough surface profiles at fixed frequency *Inverse Problems* **22** 939–54

[BF97] Burden R and Faires J D 1997 *Numerical Analysis* 6th edn (Pacific Grove, CA: Brooks/Cole)

[Bou03] Bouchon M 2003 A review of the discrete wavenumber method *Pure Appl. Geophys.* **160** 445–65

[BR92] Bruno O P and Reitich F 1992 Solution of a boundary value problem for the Helmholtz equation via variation of the boundary into the complex domain *Proc. R. Soc. Edinburgh* A **122** 317–40

[BR93a] Bruno O P and Reitich F 1993 Numerical solution of diffraction problems: a method of variation of boundaries *J. Opt. Soc. Am.* A **10** 1168–75

[BR93b] Bruno O P and Reitich F 1993 Numerical solution of diffraction problems: a method of variation of boundaries: II. Finitely conducting gratings, Padé approximants, and singularities *J. Opt. Soc. Am.* A **10** 2307–16

[BR93c] Bruno O P and Reitich F 1993 Numerical solution of diffraction problems: a method of variation of boundaries: III. Doubly periodic gratings *J. Opt. Soc. Am.* A **10** 2551–62

[CG11] Chorfi L and Gaitan P 2011 Reconstruction of the interface between two-layered media using far-field measurements *Inverse Problems* **27** 075001

[CK98] Colton D and Kress R 1998 *Inverse Acoustic and Electromagnetic Scattering Theory* 2nd edn (Berlin: Springer)

[CM85] Coifman R and Meyer Y 1985 Nonlinear harmonic analysis and analytic dependence *Pseudodifferential Operators and Applications (Notre Dame, IN, 1984)* (Providence, RI: American Mathematical Society) pp 71–8

[CS93] Craig W and Sulem C 1993 Numerical simulation of gravity waves *J. Comput. Phys.* **108** 73–83

[CSS97] Craig W, Schanz U and Sulem C 1997 The modulation regime of three-dimensional water waves and the Davey–Stewartson system *Ann. Inst. Henri Poincaré* **14** 615–67

[GR87] Greengard L and Rokhlin V 1987 A fast algorithm for particle simulations *J. Comput. Phys.* **73** 325–48

[HN05] Bei H and Nicholls D P 2005 Analyticity of Dirichlet–Neumann operators on Hölder and Lipschitz domains *SIAM J. Math. Anal.* **37** 302–20

[HN10] Bei H and Nicholls D P 2010 The domain of analyticity of Dirichlet–Neumann operators *Proc. R. Soc. Edinburgh* A **140** 367–89

[KFI04] Koketsu K, Fujiwara H and Ikegami Y 2004 Finite-element simulation of seismic ground motion with a voxel mesh *J. Pure Appl. Geophys.* **161** 2183–98

[KT00] Kress R and Tran T 2000 Inverse scattering for a locally perturbed half-plane *Inverse Problems* **16** 1541–59

[KT02a] Komatitsch D and Tromp J 2002 Spectral-element simulations of global seismic wave propagation: I. Validation *Geophys. J. Int.* **149** 390–412

[KT02b] Komatitsch D and Tromp J 2002 Spectral-element simulations of global seismic wave propagation: II. 3D models, oceans, rotation and self-gravitation *Geophys. J. Int.* **150** 303–18

[Mil91a] Milder D M 1991 An improved formalism for rough-surface scattering of acoustic and electromagnetic waves *Proc. SPIE* **1558** 213–21

[Mil91b] Milder D M 1991 An improved formalism for wave scattering from rough surfaces *J. Acoust. Soc. Am.* **89** 529–41

[Mil96a] Milder D M 1996 An improved formalism for electromagnetic scattering from a perfectly conducting rough surface *Radio Sci.* **31** 1369–76

[Mil96b] Milder D M 1996 Role of the admittance operator in rough-surface scattering *J. Acoust. Soc. Am.* **100** 759–68

[MN11] Malcolm A and Nicholls D P 2011 A field expansions method for scattering by periodic multilayered media *J. Acoust. Soc. Am.* **129** 1783–93

[MRE07] Moczo P, Robertsson J O A and Eisner L 2007 The finite-difference time-domain method for modeling of seismic wave propagation *Adv. Geophys.* **48** 421–516

[MS91] Milder D M and Sharp H T 1991 Efficient computation of rough surface scattering *Mathematical and Numerical Aspects of Wave Propagation Phenomena (Strasbourg, 1991)* (Philadelphia, PA: SIAM) pp 314–22

[MS92] Milder D M and Sharp H T 1992 An improved formalism for rough surface scattering: ii. Numerical trials in three dimensions *J. Acoust. Soc. Am.* **91** 2620–6

[NR01] Nicholls D P and Reitich F 2001 A new approach to analyticity of Dirichlet–Neumann operators *Proc. R. Soc. Edinburgh* A **131** 1411–33

[NR03] Nicholls D P and Reitich F 2003 Analytic continuation of Dirichlet–Neumann operators *Numer. Math.* **94** 107–46

[NR04a] Nicholls D P and Reitich F 2004 Shape deformations in rough surface scattering: cancellations, conditioning and convergence *J. Opt. Soc. Am.* A **21** 590–605

[NR04b] Nicholls D P and Reitich F 2004 Shape deformations in rough surface scattering: improved algorithms *J. Opt. Soc. Am.* A **21** 606–21

[NT08] Nicholls D P and Taber M 2008 Joint analyticity and analytic continuation for Dirichlet–Neumann operators on doubly perturbed domains *J. Math. Fluid Mech.* **10** 238–71

[NT09] Nicholls D P and Taber M 2009 Detection of ocean bathymetry from surface wave measurements *Euro. J. Mech. B/Fluids* **28** 224–33

[Pet80] Petit R (ed) 1980 *Electromagnetic Theory of Gratings* (Berlin: Springer)

[Pra90] Pratt R G 1990 Frequency-domain elastic wave modeling by finite differences: a tool for crosshole seismic imaging *Geophysics* **55** 626–32

[SSPRCP89] Sanchez-Sesma F J, Perez-Rocha E and Chavez-Perez S 1989 Diffraction of elastic waves by three-dimensional surface irregularities: part II *Bull. Seismol. Soc. Am.* **79** 101–12

[Zie77] Zienkiewicz O C 1977 *The Finite Element Method in Engineering Science* 3rd edn (New York: McGraw-Hill)